Available online at www.sciencedirect.com

jmr&t Journal of Materials Research and Technology

journal homepage: www.elsevier.com/locate/jmrt

Automotive brake friction composite materials using natural *Grewia Optiva* fibers

Tej Singh [a,*], *Gustavo da Silva Gehlen* [b,1], *Ney Francisco Ferreira* [b,1], *Liu Yesukai de Barros* [b,1], *Germano Lasch* [b,1], *Jean Carlos Poletto* [b,1], *Sharafat Ali* [c], *Patric Daniel Neis* [b,1]

[a] *Savaria Institute of Technology, Faculty of Informatics, ELTE Eötvös Loránd University, Szombathely, Hungary-9700*

[b] *Laboratory of Tribology, Federal University of Rio Grande Do Sul, Osvaldo Aranha, 99, Porto Alegre, Brazil*

[c] *Allied Nippon Private Limited, Sahibabad, U.P., India-201010*

ARTICLE INFO

Article history:
Received 17 May 2023
Accepted 7 September 2023
Available online 12 September 2023

Keywords:
Natural fiber
Grewia optiva
Brake material
Fade-recovery
Stick-slip

ABSTRACT

There have been growing concerns over using non-renewable resources while manufacturing goods and related environmental laws worldwide. As part of efforts to reduce dependence on non-renewable resources, the uses of natural resources in brake friction materials are gaining prominence. Therefore, a natural fiber from the Himalayan region, *Grewia Optiva*, was used in the present study to develop a sustainable material for automotive braking applications. Brake friction composite materials were manufactured with various amounts (0, 2.5, 5, 7.5, and 10 wt%) of *Grewia Optiva* fiber. The composites were evaluated for physicochemical and mechanical characterization, tribological properties, and noise propensity. The friction performance remains comparable for all composites between 0.41 and 0.44, while a 9–13% reduction in the specific wear rate was obtained for the ≥7.5 wt% *Grewia Optiva* fiber added to the composites. Fade-recovery performance improved significantly with increasing fiber amount, while friction fluctuations remained the lowest for the composite with 7.5 wt% *Grewia Optiva* fiber content. At the same time, the minimal stick-slip power was associated with the composite having no *Grewia Optiva* fiber content. Therefore, a multiattribute decision-making technique was employed to evaluate the overall performance of all the composites suggesting 7.5 wt% *Grewia Optiva* fiber as the optimal content.

1. Introduction

Undeniably, the last few decades witnessed a massive surge in research highlighting the beneficial role of natural fibers in various applications. This is a breakthrough in technology as natural fibers are considered an eco-friendly approach, contributing to the global effort to protect the environment from further damage by pollutants caused by synthetic materials [1]. The United Nations set 17 goals for sustainable development in the 2030 agenda, two of which are responsible

* Corresponding author.
E-mail address: sht@inf.elte.hu (T. Singh).
[1] www.ufrgs.br/latrib

https://doi.org/10.1016/j.jmrt.2023.09.072

consumption and production (Goal 12) and climate action (Goal 13) [2]. Natural fiber-based products will help meet a green society's sustainable development goals and vision. According to the 2019 "EU Green Agreement," carbon dioxide emissions must be reduced by 50–55% by 2030 compared to 1990 to achieve carbon neutrality by 2050 [3]. In line with this, not only is the carbon footprint of natural fibers reported to be one-third that of synthetic fibers, but it is approximately 20–50% less for natural fiber-reinforced composites than that of synthetic fiber-reinforced composites [4,5]. As a result of environmental conservation, global industries have focused on natural fibers to achieve a positive balance between the economy and the environment by manufacturing green products [6]. Green products are intended to save resources or energy, poses less harm to the environment, and provides consumers and society with a higher living standard. Nowadays, consumers have become more sensitive to the environmental impact of their purchases and are willing to buy green products at a higher price than conventional products [7].

One of the green products based on natural fibers is automotive brake friction composite materials [8]. Using natural fibers helps reduce carbon emissions and opens up possibilities for brake composite production while avoiding synthetic materials [9]. Several exciting studies have shown using natural fibers to develop friction materials. Some used banana, pineapple, hemp, ramie [10], jute [11], kenaf [12], flax [13], abaca [14], corn stalk [15], rice-husk [16] and cow dung [17] fibers. Most of those studies on the role of green brake materials focused between 5 and 20 wt% of natural fiber content. It was concluded that the friction and wear properties remain optimal for the brake material with natural fiber content of 5–10 wt%. The high dosages (>10 wt%) were reported deteriorating the tribological performance due to the lower thermal stability of natural fibers. For example, in [10,18], increasing the amount of natural fibers above 10 wt% resulted in increased friction instability, as well as a significant decrease in temperature-sensitive braking performance, which is mainly due to thermal degradation of natural fibers.

In addition, the increasing relevance of ecology is forcing industries to reduce brake emissions and produce environmentally friendly friction composite materials [19–21]. Song et al. [22] investigated the effect of various types of fibers (steel, cellulose, mineral, and aramid) on automotive brake friction composites. The study concluded that cellulose, which contains natural polysaccharides, proved to be equally good as aramid in reducing brake emissions by escalating the friction films on the composite surface and improving wear resistance. The recent studies by Monreal-Perez et al. [23] claimed that brake materials reinforced with sheep wool showed good tribological performance and superior environmental performance compared to other organic fibers. These two aforementioned studies [22,23] strongly suggest that incorporating natural fibers provides a good balance between reduced airborne particulate emissions, reduced cost, increased wear resistance, and decreased environmental impact, which shows that they may become an attractive and durable material in the development of brake friction composites.

Before claiming an efficient, sustainable brake material, it is necessary to study other criteria, such as performance (friction and wear) and also comfort aspects, such as brake creep-groan noise. The friction materials are designed for safe and comfortable automobile stops but often produce annoying noise known as brake creep-groan [24]. In general, stick-slip between the contacting materials of the braking system (i.e., disc and friction material) is considered the most prominent mechanism for the occurrence of creep-groan [25]. Moreover, creep-groan symptoms during braking reduce the brand value and lead vehicle owners to lodge complaints against the automobile/friction material manufacturer, due to which industries have to spend a massive amount of money on repair and warranty costs. It is estimated that the associated annual charge to cover issues related to the noise and vibration of the braking system exceeds US$100 million [26]. Various experimental and numerical studies have been done to study the creep groan problem. In [27], brake creep-groan measured in vehicle tests was correlated to friction induced phenomenon (stick-slip) obtained experimentally through a laboratory tribometer. The researchers also proposed a new parameter to quantify the intensity of stick-slip: the slip power. According to the study, slip power represents the amount of energy that is accumulated during the stick phase, which is dissipated in the slip phase. For this reason, the authors considered slip power as the most accurate parameter to quantify the intensity of stick-slip measured in tribotests carried out in laboratory. Other studies also explore the possibility of using damping shim/insulator bonded in the brake pad as a way to reduce brake noise [28]. Some researchers changed the brake material composition and concluded that noise and vibration could be suppressed using ceramic [29] or a mixture of Zylon and aramid fibers [30] without affecting braking performance. Nevertheless, there still needs to be a study on the brake noise generated when using friction materials containing natural fibers. It is worth noting that good performance (friction and wear) allied to a reduced level of brake noise are both required outputs expected from a brake friction material.

Current publications regarding the effects of using natural fibers are mostly limited to replacing organic fibers such as aramid [31,32]. In contrast, the synergistic effect of natural fibers with other reinforcing fibers (e.g., metal and ceramic) also needs to be covered. In general, adding one fiber to the friction material does not result in satisfactory braking performance, which may further deteriorate due to the low thermal stability of natural fibers [18,33]. However, combining natural fibers with highly thermally resistant fibers (ceramic, for instance) may appear to be a beneficial approach. Nevertheless, research on how natural and highly heat-resistant fiber combinations affect friction material braking effectiveness has yet to be published. The advantages of a combination of natural fiber and ceramic fiber in automotive brake materials are yet to be investigated. Since ceramic fibers are renowned for their inherent hardness and thermal resilience, their combination with natural fiber might offer enhanced high-temperature friction performance [29,34]. The present research work, therefore, explores the use of natural fibers (*Grewia optiva*) in automotive brake friction formulations in various combinations with ceramic fibers. The fiber-producing *Grewia optiva* tree is a member of the Tiliaceae family [35]. A typical-sized deciduous tree with a stature of 9–15 m, *Grewia optiva* is primarily found in the Himalayan region [36]. The fibers of *Grewia optiva* are classified as bast fibers, which are situated in the bast region of the plants [37]. Various bast fibers, such as jute, ramie, kenaf, hemp, flax etc., were reported to be used in automotive brake friction materials [10–13]. The *Grewia optiva* tree, originating from the Himalayas, has many functions and is mainly used as a feed source for many animal species. Its cellulosic fibers, fuelwood, and edible natural products provide many applications, including their potential usage as a hair cleanser, clothing cleaning, and herbal remedies [36,37]. Furthermore, the fibers derived from the *Grewia optiva* plant are used by indigenous populations for the production of many commodities, including ropes, mats, bags, boots and socks etc. [36–38]. Consequently, these fibers have significant economic value within local economies. The wood of *Grewia optiva* is semi-hard, strong and elastic [37,38]. Older twigs of *Grewia optiva* are used to make handles for shovels, spades, axes, and light agricultural equipment, highlighting its mechanical strength [35–38]. Kalauni and Pawar [39] assessed the sound absorption coefficient of several synthetic materials, including polyurethane foam, melamine foam, and mineral wool. They also examined the sound absorption properties of natural fibers such as coir, kenaf, and *Grewia Optiva*. The study's findings indicate that the sound absorption coefficient of *Grewia Optiva* fiber is comparable to, or superior to, other synthetic and natural materials used for sound absorption. Therefore, using *Grewia Optiva* fibers as an alternative to conventional sound absorbers has the potential for practical sound absorption applications. Additionally, it has been observed that the fiber derived from *Grewia optiva* has favourable thermal stability. Furthermore, including this fiber has positively impacted polymeric composites' wear and mechanical characteristics [35–38]. Therefore, brake friction composites containing a varying proportion of *Grewia optiva*/ceramic fibers (0/10, 2.5/7.5, 5/5, 7.5/2.5, and 10/0 by weight) were fabricated and evaluated for tribological performance and propensity to brake creep-groan noise by following SAE J2522 standard test procedure.

2. Materials and methods

2.1. Materials

Phenolic resin (JA 10 grade) used as the binder for composite fabrication was obtained from Apex Phenolics, Delhi, India. Barium sulfate and synthetic graphite were purchased from Sky Minerals (Delhi, India), while exfoliated vermiculite was supported by Bharat Industries (Delhi, India). Alumina and steel fibers were purchased from Hindalco Industries (Delhi, India) and Sarda Industries (Delhi, India), respectively. Lapinus fiber was purchased from Lapinus Intelligent (Delhi, India), while ceramic fiber was supplied by Murugappa Morgan Thermal Ceramics Limited (Chennai, India). The *Grewia optiva* was supplied by local farmers of Dehlwin village (Himachal Pradesh, India). The procured *Grewia optiva* fiber was manually cut down to fiber lengths ranging from 2 to 6 mm and used without further treatment. The images (optic and SEM) of the *Grewia optiva* fiber are presented in Fig. 1. The Shimadzu TA-60WS device was used to examine the thermal stability of the ceramic and *Grewia optiva* fibers. With a 50 ml/min flow rate and a 10 °C/min heating rate in the air environment, the thermal stability was measured over the temperature range of 30 °C–800 °C. According to the findings in Fig. S1 (supplementary information), *Grewia optiva* completely degraded at 450 °C while ceramic fiber only exhibited 1% degradation at 800 °C.

2.2. Sample preparation

Five friction composites were created with a fixed composition (90 wt%) of seven ingredients. The remaining 10 wt% was modified using the *Grewia optiva* and ceramic fiber variations shown in Table 1. A high rotation shear mixer (Fabdecon Engineers, India) with a chopper speed of 3000 rev/min is used to combine the components successively. First the fibrous elements are combined with phenolic resin for 5 min, followed by powdered ingredients for another 5 min to achieve homogenous dispersion. After that, 80 g of the prepared mixture was placed in an iron mold cavity containing an adhesive-coated steel plate. The ready mold is then heated in a compression-molding machine (Fabdecon Engineers, India) with a pressure of 150 bar at 155 °C for 8 min. Four intermittent breathing cycles were employed during compression molding to remove the volatiles produced during cure. The cured composites were cooled down at room temperature and, after removal from the mold, were again cured in an oven at 160 °C for 3h. After post-curing, the composites were used for various characterizations. Based on the formulation of the materials, they can be classified as low-metallic friction materials. For the tribological study (tribotests) of the composites, a pin-shaped specimen with a diameter of 14 mm was machined

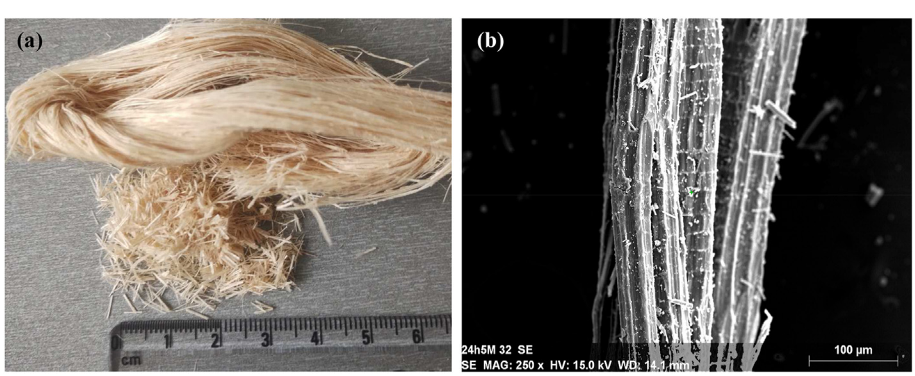

Fig. 1 – (a) Optic and (b) SEM images of *Grewia optiva* fiber.

Table 1 – Nomenclature and ingredients of the composites.

Type	Ingredients (wt.%)	Dimensions	Nomenclature				
			GF0	GF1	GF2	GF3	GF4
Binder	Phenolic resin	200 mesh	10	10	10	10	10
Fillers	Barium sulfate	325 mesh	50	50	50	50	50
	Vermiculite	40 mesh	5	5	5	5	5
Property modifiers	Alumina	325 mesh	3	3	3	3	3
	Graphite	100 mesh	6	6	6	6	6
Fibers	Steel fiber	Diameter = 175 ± 25 μm; Length = 1–2 mm	6	6	6	6	6
	Lapinus fiber	Diameter = 5 μm; Length = 175 ± 25 μm	10	10	10	10	10
	Ceramic fiber[a]	Diameter = 3–6 μm; Length = 45±3 μm	10	7.5	5	2.5	0
	Grewia optiva fiber	Length = 2–6 mm Diameter = 100 ± 25 μm	0	2.5	5	7.5	10

[a] Composition: SiO_2 = 62–68%, CaO = 26–32%, MgO = 3–7%, others<1%.

from a prepared composite. Then, the pin specimen was glued to a backplate. Gray cast iron, which is the most widely used material in brake system rotors, was used in the experiments as counterface material (disc). Fig. 2 shows a photo of an exemplary of the composite (pin) and rotor (disc) used in the tribotests.

2.3. *Physicochemical and mechanical characterization*

The produced composites were evaluated for various properties per the published industry standards [40,41]. The porosity of the composites was assessed using the JIS D 4418 standard, and the density was calculated using the conventional water displacement method. The hardness of the composites was measured with a steel ball indenter of 12.5 mm diameter on a Rockwell hardness tester, according to ASTM D 785. The quantity of uncured resin was estimated using the acetone extraction method (ASTM D494 standard). The water and heat swelling of the composites was measured as per IS2742 Part-3 of 1994 Indian standards. For loss on ignition, ~10 g of composite sample was roasted at 800 °C for 2 h in a muffle furnace. Following ISO 6312 guidelines, the shear strength contributing to the adhesion of friction material with steel back plate was assessed using a hydraulically powered setup. Utilizing ISO 6310 criteria, the compressibility of the produced composites was evaluated.

2.4. *Tribological evaluation*

The tests were performed in a laboratory-scaled brake tribometer (LSBT). This device mimics the contact pressure, velocity, and temperature seen in real-world automotive braking systems [42]. An induction heating system has been connected to the LSBT in order to regulate the starting temperature of each braking action. For disc temperature tracking, a K-type thermocouple was inserted 1.5 mm below the disc's surface at the center of the friction track. In the LSBT, the coefficient of friction (μ), as shown in Eq. (1):

$$\mu = \frac{T}{F_N \times R} \quad (1)$$

Here: T = braking torque (Nm), R = track radius (m), F_N = normal load (N) exerted by the composite sample on the disc. According to [42], the accuracy of the LSBT in terms of μ is ±0.013. The tests were carried out in line with SAE J2522 (AK Master) brake pad specifications [43]. This method is

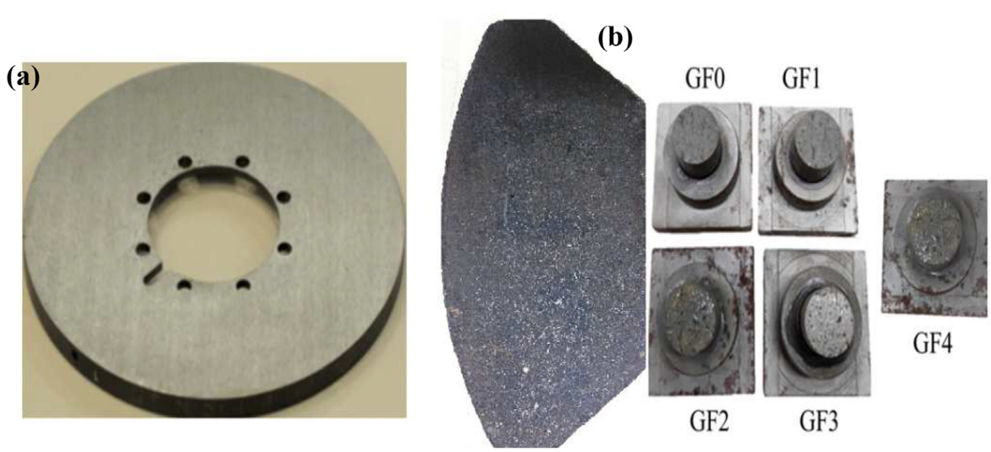

Fig. 2 – Specimens used during the tests: (a) gray cast iron disc, (b) samples (pins) of the brake friction materials.

employed by the global brake industry to evaluate the performance of friction materials under various scenarios. The stages of this method are listed in Table 2. Three samples of each formulation were subjected to the AK Master test, totalizing 15 tests.

The composites recorded μ in the fade and recovery stages was assessed by calculating recovery-% and fade resistance-% (FR-%) using the metrics shown in Eq. (2) and Eq. (3), respectively [18]:

$$\text{Recovery} - \% = \frac{\mu_R}{\mu_P} \times 100 \quad (2)$$

$$\text{FR} - \% = \frac{\mu_F}{\mu_P} \times 100 \quad (3)$$

Here, μ_P is the performance friction coefficient, calculated as an average friction obtained in the characteristic and recovery sections; μ_F is the lowest friction coefficient for the fade section, and μ_R is the average friction for the respective recovery section. These metrics are often used in research [17,44] to evaluate how brake friction materials behave, and for both parameters (FR-% and recovery-%), the higher result denotes the best performance. By subtracting the mass of each sample before and after the tribological tests, wear of the samples was determined through mass loss. The samples were weighed using an electronic balance with an accuracy of 0.1 mg. According to Eq. (4), the specific wear rate (SWR; cm^3/Nm) of the composites was determined.

$$\text{SWR} = \frac{\Delta W}{\rho \times F \times S} \quad (4)$$

Here, ΔW = specimen weight loss (g), ρ = specimen density (g/cm^3), S = sliding distance (m) and F = friction force (N). Micrographs of the specimen's surface (4.2 × 3.2 mm) in the middle were acquired using an optical microscope (with a digital CMOs camera mounted in a Carls Zeiss model Axio Lab. A1). The worn surfaces contact plateaus were estimated in nominal area (%) using MATLAB software based on Otsu's technique [45]. Also, through a stereoscope Zeiss model Stemi 508, the macroscopic surface condition of the specimens was evaluated before and after the tests. To assess the development of tribofilm on the brake disc's surface after each braking action, photos of the surface were taken. The photographs were taken with a 24.2 megapixel resolution digital camera (Canon EOS Rebel T6i) and a Macro USM lens (Canon EF 100 mm f/2.8). An LED light ring was also used to sufficiently illuminate the disc's surface. After each braking action, the tribofilm on the disc surface was measured using a specific MATLAB technique. The quantity of tribofilm in each friction track's picture was determined using the average pixel intensity, which ranges from 0 to 255. To investigate the homogeneity of the tribofilm distributed across the disc, the pixel intensity of the pictures was also analyzed in the radial direction.

To verify the susceptibility to low frequency brake noise, an analysis of the stick-slip phenomenon was performed immediately after the AK Master test, enabling a more reliable assessment of the friction material's performance since the material had already passed through a thermal-load condition. Table 3 presents the conditions of the stick-slip experimental procedure. A test cycle consists of a normal force starting at 1000 N, which is linearly reduced to zero in 100 s, with the disc rotating at 0.5 rev/min. Thirty cycles were performed for each sample. The driver of a car slowly releasing the brake pedal is equivalent to this normal force reduction. The sensors installed on the testing machine (encoder, torque transducer, and others) recorded a multitude of stick-slip events as the force reduction took place. The analysis of the stick-slip results was done by the traditional comparison between static and dynamic friction values, as seen in several studies [25–27], and by the slip power parameter. This last parameter considers the amount of energy dissipated by time and has already been presented and validated with results by this research group in a previous work [27].

Table 2 – SAE J2522 test procedure.

Section	Pressure [bar]	Initial brake temperature [°C]	Brake-release speed [km/h]	Number of applications [–]
Green characteristic	30	100	80–30	30
Burnish	15–51	100	80–30	64
Characteristic value	30	100	80–30	6
Speed/pressure sensitivity (SPS)	10–80	100	40–5	8
			80–40	8
			120–80	8
			160–130	8
			200–170	8
Characteristic value	30	100	80–30	6
Cold	30	40	40–5	1
Characteristic value	30	100	80–30	18
Fade 1	0.4 g (deceleration)	100–550	100–5	15
Recovery 1	30	100	80–30	18
Temperature/pressure sensitivity (TPS)	10–80	100	80–30	8
	30	100–500		9
	10–80	500		8
Recovery 2	30	100	80–30	18
Fade 2	0.4 g (deceleration)	100–550	100–5	15
Recovery 3	30	100	80–30	18

Table 3 – Parameters of the experimental procedure for stick-slip evaluation.

Speed (rev/min)	Normal force (N)	Force reduction rate (N/s)	Time (s)	Replication
0.5	1000	10	100	30

2.5. *Multiattribute performance evaluation*

A widely recognized weighted linear scoring method, namely simple additive weighting (SAW), has been used to rank the composites. SAW is one of the most applicable multi-attribute decision-making methods due to its simple procedure [46]. Each composite's assessment score is calculated for ranking purposes by multiplying its normalized value by the weighted relevance of each characteristic. The assessment score of different composites was calculated after constructing an assessment matrix for the alternatives (m) and attributes (n) by employing the following equations [46].

$$\text{Assessment matrix} = (A_{ij})_{m\times n} \tag{5}$$

$$\text{Assessment score, } A_s = \sum_{j=1}^{n} W_j (A_{ij})_{normal} \tag{6}$$

where W_j represents the weighted relevance; in this study, equal weights were assigned to each attribute; The normalized assessment matrix $(A_{ij})_{normal}$ is determined based on the implications (beneficial, i.e., higher-the-better, and in case of non-beneficial, i.e., lower-the-better) of the selected attributes, as shown by Eq. (7).

$$(A_{ij})_{normal} = \begin{cases} \dfrac{A_{ij}}{\max(A_{ij})} & if\ j \in eneficial\ attribute \\ \dfrac{\min(A_{ij})}{A_{ij}} & if\ j \in non-beneficial\ \ attribute \end{cases} \tag{7}$$

3. Results and discussion

3.1. *Results of the physicochemical and mechanical properties*

The composite samples were characterized for various properties per industrial standards, and the corresponding results are listed in Table 4. The densities of these composites decreased with the increasing content of *Grewia optiva* fibers.

Table 4 – Results of various characterizations.

Properties	GF0	GF1	GF2	GF3	GF4
Density [g/cm^3]	2.49	2.470	2.45	2.43	2.42
Hardness [HRR]	92	89	87	84	82
Uncured resin [%]	0.12	0.18	0.32	0.28	0.34
Porosity [%]	4.34	4.56	5.12	5.32	5.88
Compressibility [%]	1.26	1.29	1.31	1.35	1.41
Shear strength [kgf/cm^2]	48.54	46.19	45.99	44.97	44.66
Heat swelling [mm]	0.03	0.03	0.04	0.04	0.04
Water swelling [mm]	0.04	0.04	0.04	0.05	0.05
Loss on ignition [%]	19.2	21.8	24.2	26.6	28.9

The sample GF0 had the highest density (2.49 g/cm^3), and sample GF4 had the smallest density (2.42 g/cm^3) of all composites. This trend in density is expected as *Grewia optiva* (~1.2 g/cm^3) is a lighter ingredient, thereby reducing the density of the composites.

The hardness of the composites showed a similar tendency with an increase in the content of *Grewia optiva* fibers, i.e. it decreased as the content of *Grewia optiva* fibers increased. The decreased hardness with increased *Grewia optiva* loading was strongly correlated with reduced density. Table 2 shows the physico-chemical and mechanical properties obtained for the produced composites. The uncured resin remained within the range of 0.12–0.34% for all the friction composites and within the prescribed acceptable limit, which is described by [40]. The porosity ranges between 4.34 and 5.88%, and increased with the *Grewia optiva* fiber content. The observed trend in porosity is in accordance with the literature, which usually describes the natural fibers as porous structures [17]. The compressibility of the investigated friction composites remained in the range of 1.26%–1.41% and was found to increase with increased *Grewia optiva* fiber loading. The higher compressibility (in %) measured for the composites with greater content of *Grewia optiva* fiber can be attributed to their increased porosity values. The shear strength values depend mainly on the friction composite's interfacial bonding with the backing steel plate. All composite samples showed shear strength between 44 and 49 kgf/cm^2 with 100% coverage of friction material with the back plates. All the composites' shear strength values are above the required OEM value of 40 kgf/cm^2 [38]. The observed difference in heat and water swelling values between the compositions is negligible and does not give any specific trend on heat and water swelling with increasing *Grewia optiva* content. The loss on ignition increased with *Grewia optiva* loading. The higher content of heat-resistant ceramic fiber in GF0 and GF1 combined with the lower amount of natural fibers in those specimens helped to prevent higher values of loss on ignition.

3.2. *Tribological performance evaluation*

3.2.1. *Performance coefficient of friction*

The results of the coefficient of friction (μ) obtained from the braking tribometer for the entire SAE J2522 test procedure is depicted in Fig. 3. Some considerable changes in coefficient of friction can be seen in the speed/pressure sensitivity (SPS) section, and also from the braking #173 until the end of the test (braking #274). These brakings (#173-#274) correspond to sections related to high temperature, such as fade and temperature/pressure sensitivity (TPS). Several scenarios are described in Figs. 3–6 in terms of the dependency of friction performance on different testing settings, which correspond to the different sections of the SAE J2522 test procedure.

Fig. 4 shows the so-called performance coefficient of friction (μ_P) obtained for each sample material in the three repetitions (trial 1, trial 2 and trial 3). The μ_P was the average of μ collected during characteristic value and recovery test sections. This parameter was also used and discussed in [18]. All friction materials have nearly identical μ_P values, ranging from 0.41 to 0.44. No significant variations in μ_P were seen with increasing natural fiber loading, indicating it may be beneficial

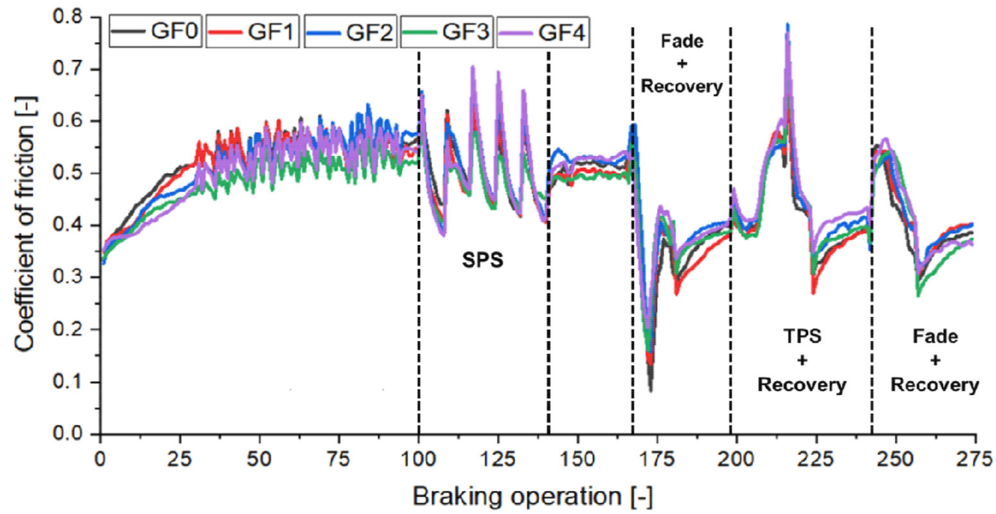

Fig. 3 – Average friction coefficient per braking operation for the entire SAE J2522 test procedure.

in combining a natural material (*Grewia optiva*) with heat-resistant fibers (ceramic).

3.2.2. *Speed-pressure sensitivity (SPS)*

One of the critical aspects of a brake material is its stability under varying speeds and applied pressure conditions. It is desired that the brake material shows as low as possible changes with speed and pressure conditions. The results of the average μ recorded during the speed-pressure sensitivity section of the SAE 2522 test procedure are presented in Fig. 5. For all brake material specimens, μ decreased with increasing pressure at all speeds. The decreasing μ with increased pressure is a disadvantage because commercial friction materials are expected to maintain a constant μ across different braking conditions. Besides, the highest magnitude of μ was observed at the lowest pressure (10 bar) for all specimens. This fall in μ with the increase in pressure is a well-known behavior of brake friction materials, as shown in [18,47].

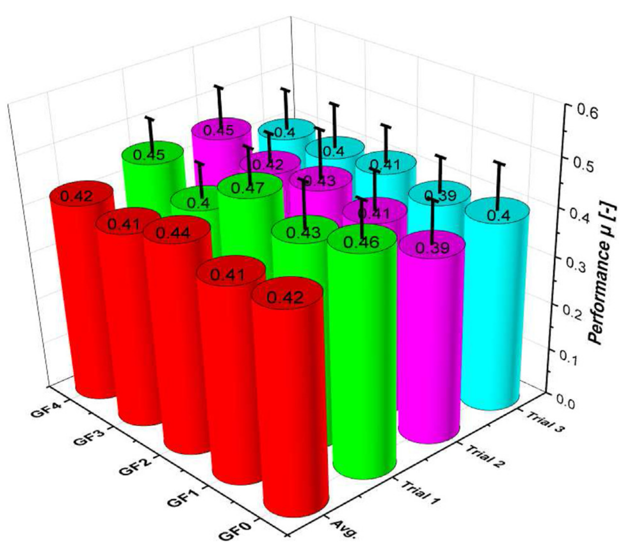

Fig. 4 – Average performance μ for different compositions.

The current data also show that μ changes with speed, although not as significantly as pressure. To assess the stability of μ in the pressure-speed sensitivity cycle, the average value of friction (μ_{avg}) was calculated for each set of speeds (40-5 km/h, 80-40 km/h and so on), as well as the amplitude/fluctuation of friction (Δμ) was obtained, the latter representing the difference between the maximum and minimum μ obtained at different speeds. The results of the analysis of the stability of μ in the pressure-speed sensitivity cycle are shown in Fig. 6.

The μ_{avg} displays almost identical trends for the tested composites at all speeds (Fig. 6a). For all composites, the μ_{avg} displayed a slight increase at mid speeds (≤120–80 km/h). This trend in μ_{avg} is a typical frictional characteristic of low-metallic frictional composites, evidenced by steel fibers (Table 1). As the speed increased (e.g., 160-130 km/h-200-170 km/h), the μ_{avg} reduced for all composites due to a phenomenon called velocity-weakening. These findings are consistent with those of Kim et al. [48] and Candio et al. [49], who found that the friction coefficient of fiber-reinforced metallic brake materials reduces as velocity increases. Regarding the friction fluctuation (Δμ) in the SPS cycle (Fig. 6b), at mid-speed block (80-40 km/h), it was noticed that Δμ remains ≤0.15 for all composites, whereas for most of the other speed blocks a higher Δμ (≥0.17) was recorded. Interestingly, for composite GF3 (2.5/7.5 wt% of ceramic and natural fiber, respectively) the Δμ was considerably lower (≤0.10), especially at higher speeds. The observed results are consistent with those of [34], where the authors also found a lower Δμ for composites combining a high content in organic fiber (≥7.5 wt %) with a reduced amount of ceramic fiber.

3.2.3. *Temperature sensitivity*

Fig. 7 displays the sensitivity of μ during the sections related to high temperature, i.e. fade and TPS, intercalated by recoveries. The fade section aims to check the loss of μ performance at high temperature, whereas its return to typical performance is assessed through the recovery section. Regarding μ recorded

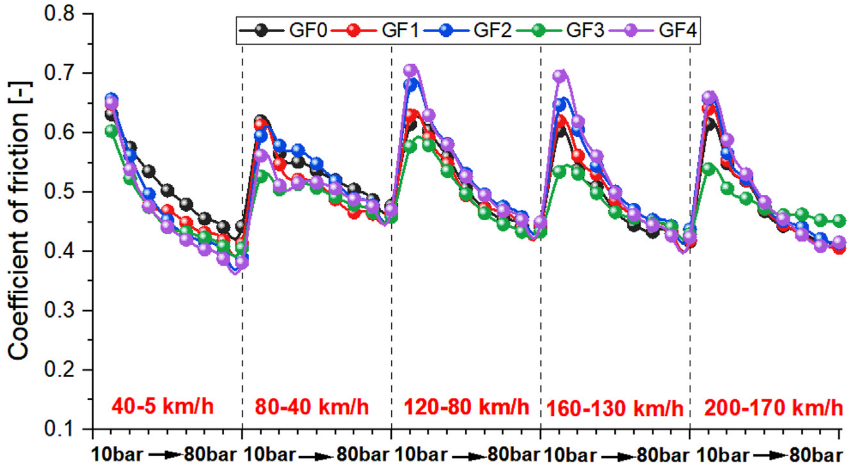

Fig. 5 – Pressure sensitivity of μ for each composition at different levels of speeds.

in fade 1, all composites showed steep μ-decay at the first brakings from #15 braking applications in the fade section. This is followed by a rapid μ-peeking at the last brakings of the fade 1. The μ-decay in fade 1 may be associated with the thermal settlement, similar to green effect of the composites, as they passed through the high-temperature phase of the test (IBT ≥100 °C) for the first time. The behavior of μ in fade 2 is different. In this case, the loss in μ is weaker compared to fade 1, and a rapid and more sustainable gain in the coefficient of friction is observed from the second braking and further.

Moreover, the composite GF0 showed the maximum fluctuation in friction ($\Delta\mu = 0.2$) during the fade 2 section. This fluctuation decreased with *Grewia optiva* fiber addition and exhibited the lowest amplitude ($\Delta\mu = 0.08$) for the GF3 composite, a beneficial feature. The μ gradually increased with increased braking applications in the recovery sections. A slight decrease in μ was seen during the pressure-rising period of the TPS section. At the temperature-rising period of the TPS, an almost constant increase in μ has occurred. This may be correlated with the disintegration of the pre-formed friction film at the previous brakings (pressure rising), which was performed at high contact pressure. This effect of film destruction in high contact pressure was previously described by Barros et al. [50]. The μ decreased with further pressure rising because of friction film formation-destruction-reformation dynamics, as will be discussed later. The summary of the fades and recoveries presented in Fig. 7 is quantified in terms of FR-% and recovery-% using the equations described in section 2.4. Higher FR-% and recovery-% are essential to obtain better performance of friction materials. A recovery of 100% is an ideal behavior since it means the brake materials recover their nominal friction level (i.e., the performance friction - μ_P). Achieving 100% fade resistance is ideal because it implies that the μ did not change with temperature. Fig. 8 presents the results of average μ in the recovery and the respective recovery percentage for all composites selected in this study. The recorded μ_R fluctuated between 0.37 ± 0.04 for all composites in all recovery sections. The μ_R values were within the expected range for a brake friction material [18]. Based on the graph of Fig. 8a, no clear relation between μ_R and

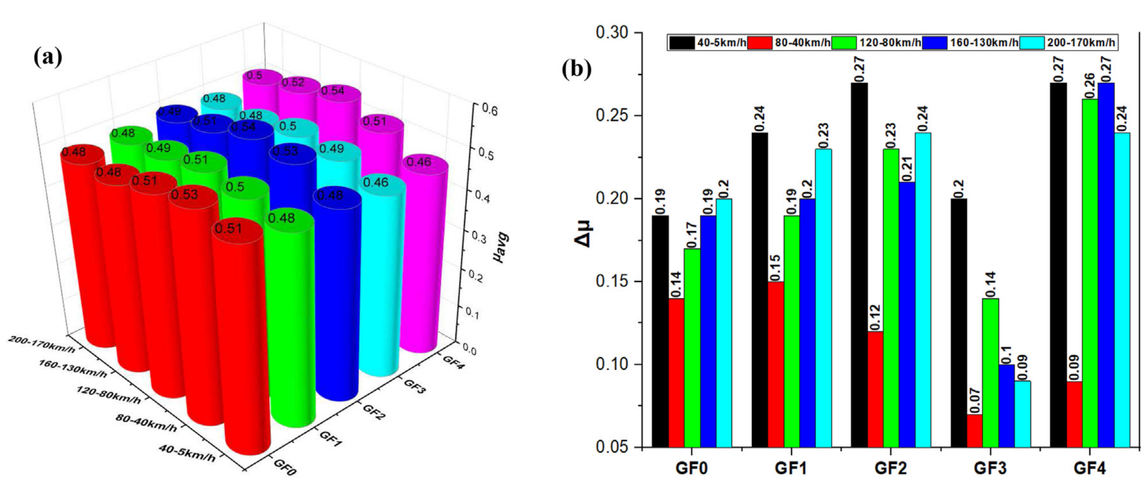

Fig. 6 – Analysis of the speed-pressure sensitivity section: (a) average value of friction (μ_{avg}) for each set of speed, and (b) friction fluctuation (Δμ) of friction for various speeds.

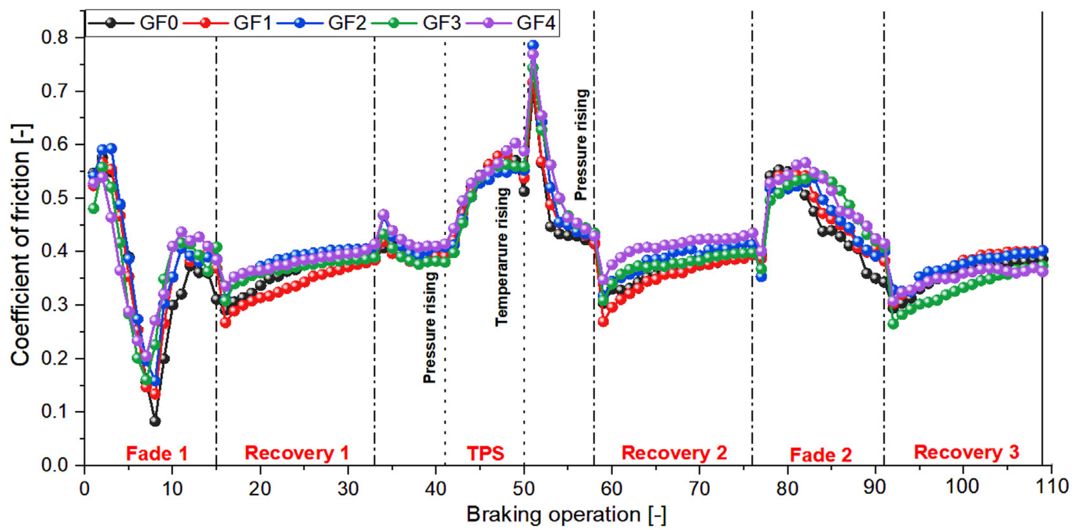

Fig. 7 – Average μ for each composition at various stages of temperature sensitivity.

natural fibre content (*Grewia optiva*) can be seen. Regarding the percentage of recovery (Fig. 8b), overall, it fluctuates between ~88 ± 7% in all recovery sections, which can be considered satisfactory.

Fig. 9 presents the results of minimal friction recorded in the fade (μ_F) and the area fraction of contact plateaus correlated to the fade resistance in fade 1 and fade 2. A gradual increase in μ_F was noted with the inclusion of *Grewia optiva* fiber, which may be ascribed to the formation dynamics of friction film at the braking interface. Regarding the FR-% shown in Fig. 9, it is seen that adding *Grewia optiva* fiber enhanced FR-% for both the fade sections, i.e., fade 1 and fade 2. Compared to fade 1, fade 2 had higher FR-% for all composites, exceeding 90% for composites with ≥7.5 wt% *Grewia optiva* content (i.e. GF3/GF4). Compared to GF0, almost 14% enhancement in fade resistance (%) was recorded for the composites having ≥7.5 wt% fiber content (i.e., GF3/GF4) during the fade 2 section. A similar result for increased fade resistance was reported in the literature for aramid [51] and natural fibers [52], ascribed to contact plateaus formation.

As hypothesized, the construction of increased contact plateaus on the composite surfaces with *Grewia optiva* fibers resulted in increased frictional performance during the fade sections. This hypothesis can be evidenced by analyzing the worn composite surfaces for contact plateaus, which are related to the actual contact area (Fig. 10).

Generally, the contact plateaus formed on worn composite surfaces are primary and secondary, which play an essential role in the stability of μ [53]. The primary contact plateaus may include wear-resistant ingredients (e.g., steel and ceramic fibers) and abrasives protruding from the surface of the composite. According to several studies, the hardened fibers

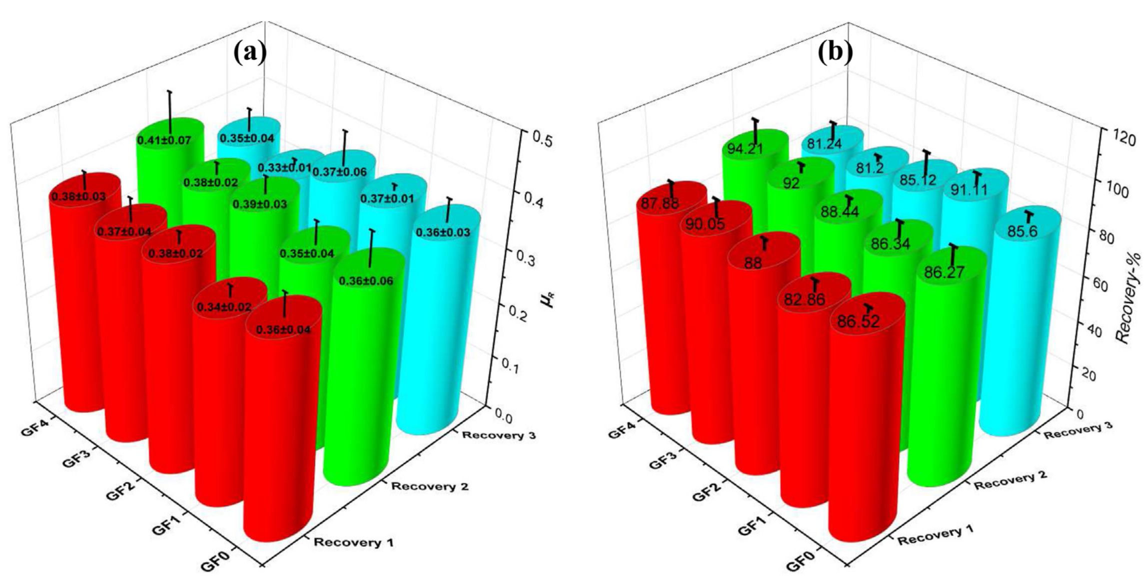

Fig. 8 – Analysis of the recovery sections, in terms of (a) average friction (μ_R), and (b) recovery-%.

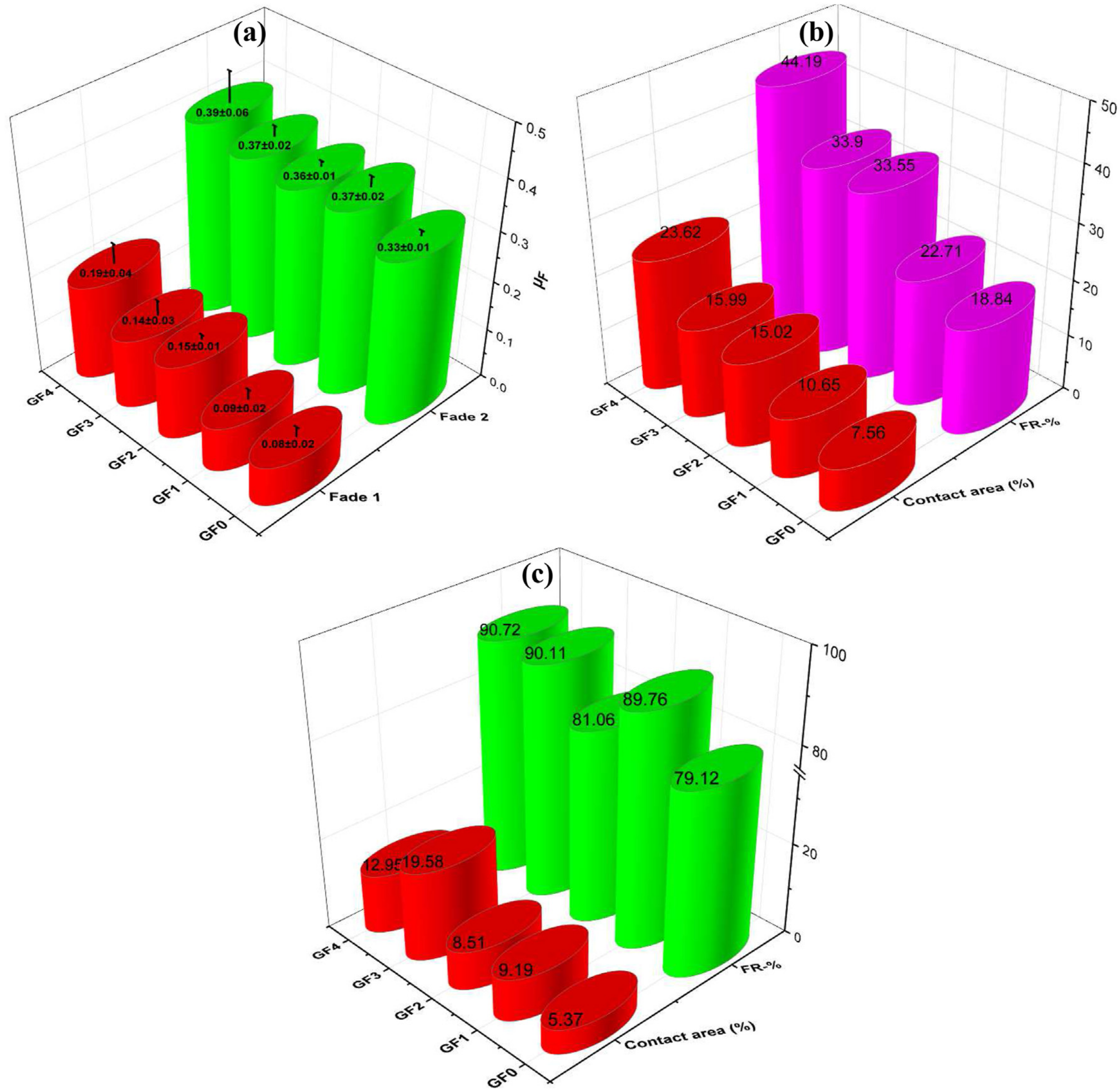

Fig. 9 – Analysis of the fades: (a) lowest friction (μ_F) in the fade sections, area fractions of contact plateaus with FR-% of the composites for (b) Fade 1, and (c) Fade 2 sections.

exposed on the composite surface aided in the production of secondary contact plateaus by enabling the build-up of wear debris behind the primary plateaus, as seen in Fig. 10. The size of secondary contact plateaus was found to increase for both fade sections and with an increase in *Grewia optiva* fiber content. This is consistent with previous research, which has shown that cohesion, agglomeration, and compaction of wear debris near primary contact plateaus encourage the creation of secondary contact plateaus [48]. The formation of secondary contact plateaus is vital for stabilizing friction performance [48]. Therefore, to elucidate the role of contact plateaus in stabilizing friction, the area of composite contact plateaus (secondary plus primary) was measured after both fade sections, and the results are shown in Fig. S2 (supplementary information). According to the worn surface microstructure, the area fraction of contact plateaus for GF0 remained low after both fade sections and increased with Grewia optiva fiber. The lower contact plateaus in GF0 decrease the total contact area, increasing the contact pressure in the few remaining contact plateaus, resulting in a significant loss in friction, as found experimentally [54]. On the other hand, contact pressure will be reduced for *Grewia optiva* fiber composites due to the increased real contact area, resulting in improved fade performance. Fig. 11 shows more clearly the difference in the amount of contact plateaus between the formulation without any natural fiber (GF0) and the formulation with higher amount of *Grewia optiva* natural fiber (GF4).

3.2.4. *Wear analysis*

The results presented in Fig. 12 represent the specific wear rate and the change in wear of the entire test procedure (SAE J2522). They revealed that the higher amount of *Grewia optiva* fiber ($\geq$7.5 wt%) is beneficial. A decrease of 9–13% in wear is seen for GF3 and GF4 in relation to GF0. For composites with $\leq$5 wt% of *Grewia optiva* fiber, specific wear rate remains higher, between $3.85 \pm 0.15 \times 10^{-7}$ cm^3/Nm. An average wear

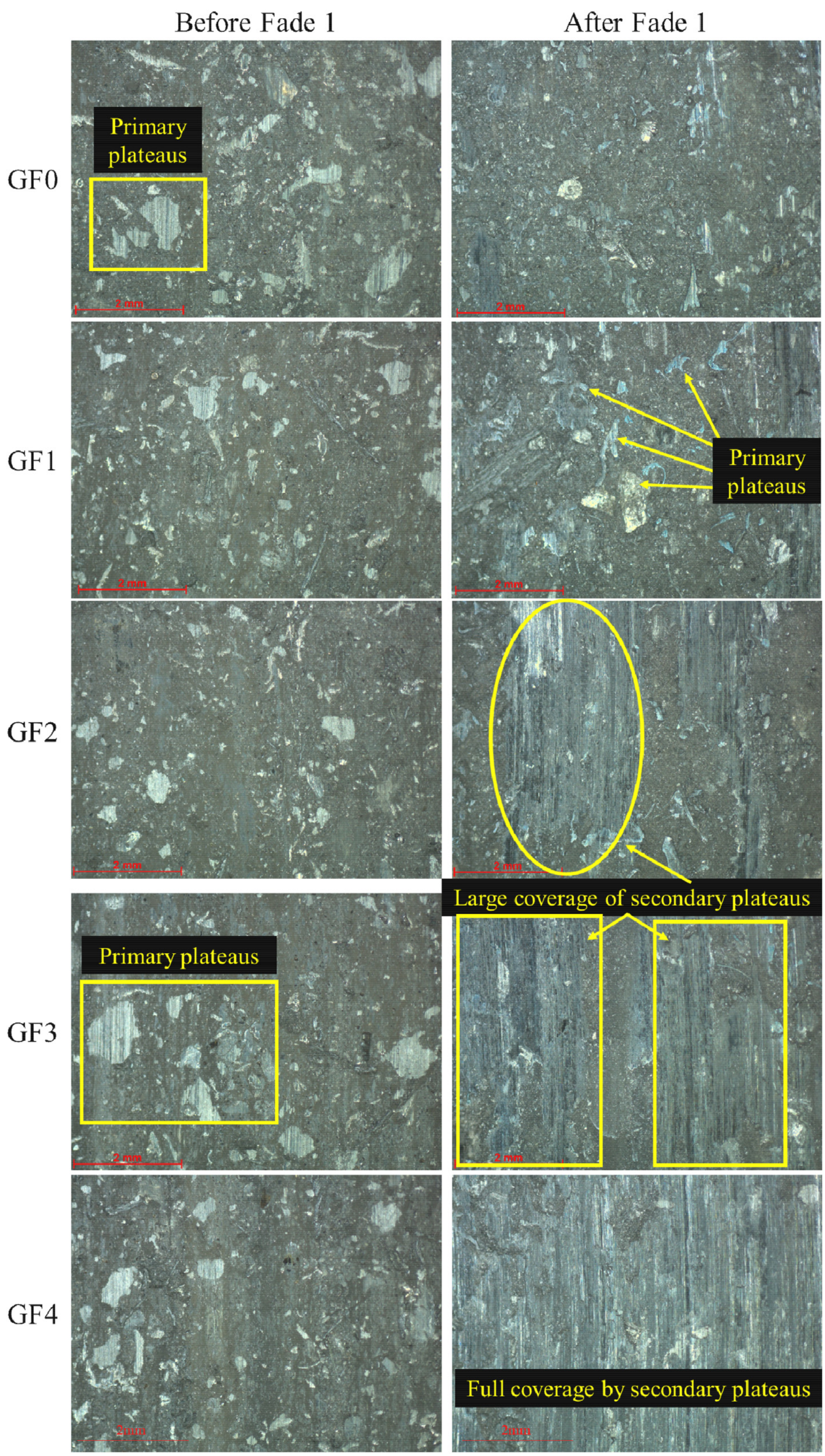

Fig. 10 – Macroscopic images of the worn surface of each formulation before and after fade 1, highlighting the formed contact plateaus (primary and secondary).

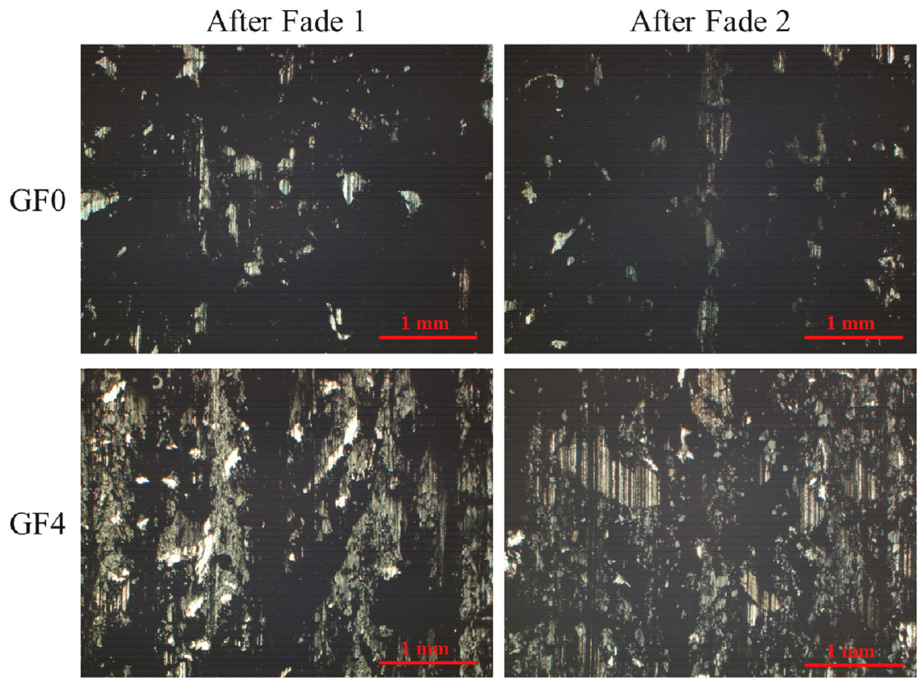

Fig. 11 – Microscopic images of the contact plateaus on the composite's surface after the fade sections.

rate of about 3.76×10^{-7} cm^3/Nm was recorded for the GF0 composite. The composite GF3 recorded the lowest wear of 3.26×10^{-7} cm^3/Nm, almost 13% smaller than the composite with pure ceramic fiber, i.e., GF0. The composites GF3 and GF4 showed the lowest wear rate, containing more natural fiber. The results correlate well with Kim et al. [55], where the authors claimed the lowest wear for the combination of aramid fiber and potassium titanate whiskers. The result also matches with the studies that included organic fiber such as aramid [50] and rice husk [18] resulted in increased wear resistance and credited to the formation of large areas of contact plateaus. The construction of contact plateaus on the composite surfaces plays a decisive role in controlling the tribological performance of any brake friction material. The lowest wear value presented by hybrid formulation GF3

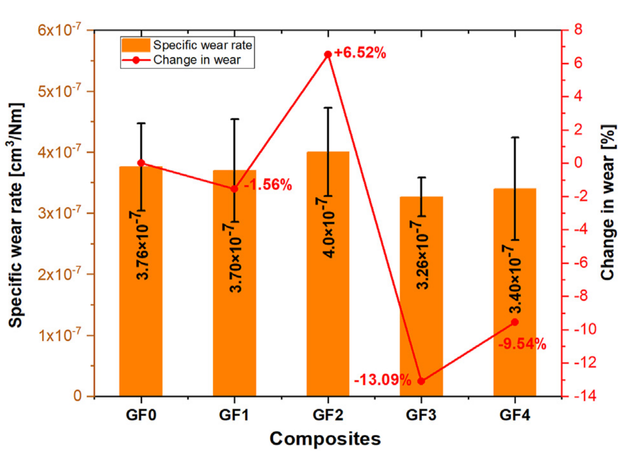

Fig. 12 – Average specific wear rate and change in wear (in relation to GF0) for each composition.

(which among hybrid formulations presents the highest amount of natural fiber) agrees with what was presented by Gehlen et al. [56], where the authors reported an improvement in wear resistance when creating hybrid composites of sisal fiber and glass fiber, resulting from the ability of sisal fiber to retain/accumulate debris from the glass fiber. The literature has reported that the wear of friction composites increases with a decrease in the formation of contact plateaus [57].

The specific wear rate and area fraction of contact plateaus of the composites are measured for high-temperature sections (fade 1, TPS and fade 2), and they are presented in Fig. 13a and a, respectively. Overall, the highest specific wear rate was recorded for TPS section. This is expected as the braking temperature reached 500 °C for fade sections while it was >500 °C during TPS section. At those temperatures (IBT≥500 °C), the organic ingredients (phenolic resins and *Grewia optiva* fiber) did not represent any advantage as they lost their thermal stability. With increased temperature, the adhesion strength of the phenolic resin decreases, making it easier for components to peel off, resulting in impaired overall wear. Regarding the area fraction of contact plateaus obtained after the fade 1 section, it was found to increase with increased *Grewia optiva* fiber content. However, the specific wear rate remains in the high temperature sections was almost the same for all composites.

As fade 1 is the first section where composites are exposed to high temperatures (up to 500 °C), it can be assumed that most of the temperature is absorbed by the composite ingredients to possible structural and chemical changes [25]. At higher temperatures, degradation of the organic material and subsequent accumulation of wear debris resulted in the formation of contact plateaus, which increased with *Grewia optiva* fiber content. Similar results have been reported in the

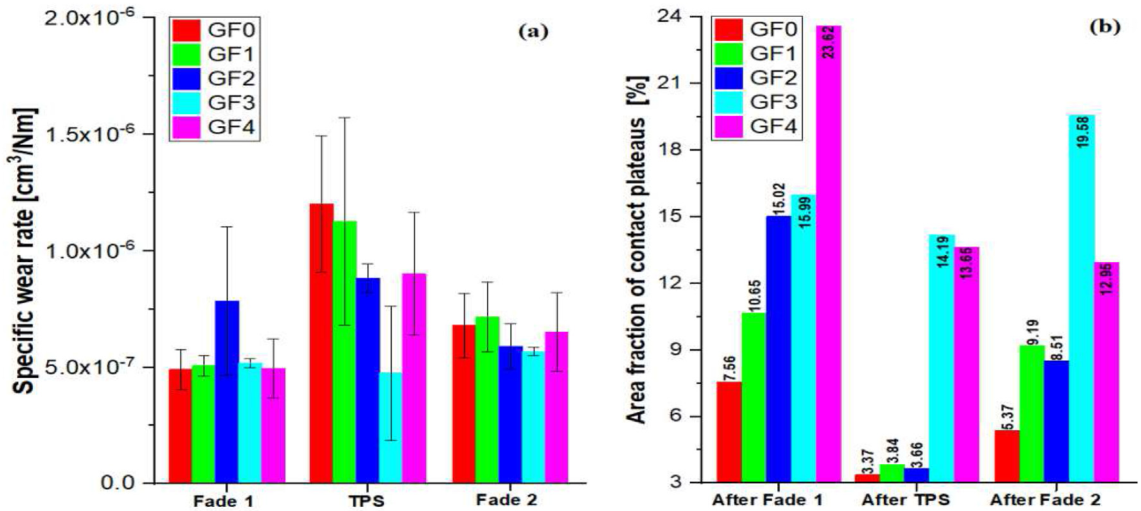

Fig. 13 – (a) Results of average specific wear rate and (b) area fraction of contact plateaus at different test sections for each composition.

literature on the role of rice husk [18] and sisal fiber [58] on the formation of contact plateaus. In [18], the real contact area increased by 40% for changing the rice husk content from 0 to 6 wt%, while the wear decreased by ~38% during the fade 1 section.

3.2.5. *Wear mechanism*

The formation-destruction-reformation of contact plateaus on the sliding surfaces determines the friction and wear performance of the composites [59,60]. Gaining a comprehensive understanding of the morphological characteristics of worn composite surfaces has significant potential in facilitating the realization of tribological properties shown by composites. During the braking process, the interaction between the composite and counter surface leads to forming a friction film. This friction film plays a crucial role in determining the overall performance of brake friction materials. The ideal outcome often involves the development of a thin, consistent, and homogenous friction film. The optimal friction film should safeguard the matrix and constituents against rapid removal during subsequent sliding. Establishing a cohesive and appropriate friction film will enhance friction's stability and reduce the wear rate [33,51]. Composite wear is associated with developing both primary and secondary contact plateaus on the surface [40,41]. The interaction between the rotating disc and fibrous ingredients leads to the creation of primary contact plateaus. Additionally, the application of braking pressure causes the wear particles to compress, resulting in the production of secondary contact plateaus. The literature has reported that these secondary contact plateaus contribute to the formation of smooth friction films on the composite surface, which may be beneficial for stabilizing friction performance with reduced wear [61].

During braking, the loosely attached ingredients are easily peeled off as small debris from the composite surface due to the contact and physical movement between the composite and counter disc. Here, it can be assumed that the dislodged ingredients can act in two ways. First, these ingredients accumulate on the composite surface to enhance the formation of secondary contact plateaus. Second, they are released as wear debris from the composite surface. The first point strongly correlates with the appearance of more secondary contact plateaus for increased *Grewia optiva* fiber-based composites. As confirmed in Fig. 10, the surfaces of composites with a lower concentration of *Grewia optiva* (i.e. GF0/GF1/GF2) exhibit a significant proportion of primary components that are exposed during the sliding process and aid in the formation of primary contact plateaus. The lack of secondary contact plateaus in these composites indicates that the surface does not contribute to the growth of the friction film through wear-particle compaction but is instead pulled out as wear debris with subsequent sliding. Such topographic features increase wear because the pulled-out debris/particles were not compressed enough to frame the secondary contact plateau/friction film [62,63]. Variations in wear mechanism were seen when *Grewia optiva* fiber concentration increased. In GF3/GF4 composites, the thin, advantageous film covers almost the whole surface, reducing the amount of exposed primary ingredients. Therefore, it can be deduced that the incorporation of higher levels of *Grewia optiva* fiber resulted in an enhancement in the quality of the produced film. This improvement substantiates the film's ability to safeguard the surface elements against further deterioration. Thus, the presence of *Grewia optiva* fiber controls and maintains the rheology cycle of the contact plateaus during brake applications.

The possible wear mechanisms identified on the samples (in order of decreasing wear resistance) are presented in Fig. 14. Before the high-temperature sections (fade), the wear regime is mild, and the surfaces of all samples consisted mainly of abrasion on the contact plateaus, as seen in Fig. 14a. In high-temperature braking, other wear mechanisms were observed (thermal damage, plateau pullout, cracks and peeling), leading to an increase in material wear. The formulations with a higher amount of *Grewia optiva* fiber (GF3 and GF4), where a large coverage of secondary plateaus was

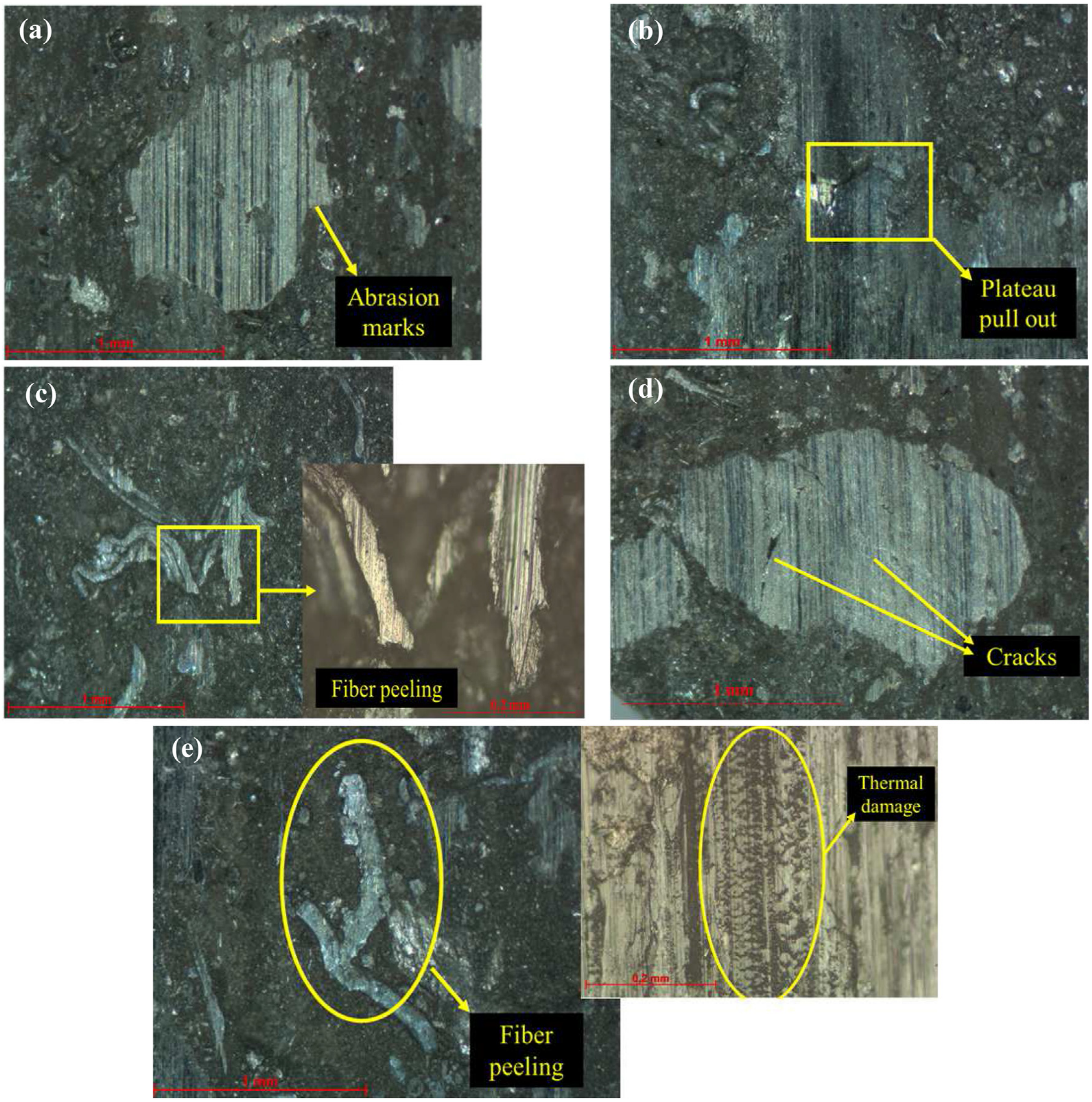

Fig. 14 – Wear mechanisms identified in the formulations before fade 1 (a) GF3; and after fade 1 (b) GF4, (c) GF1, (d) GF0, (e) GF2.

verified on their surfaces (as corroborated in Fig. 10), and exhibited removal of the formed plateaus (typical example in Fig. 14b). On the other hand, for the formulations with less natural fiber (GF0 and GF1), peeling (Fig. 14c) and the breakage (cracks on Fig. 14d) of the reinforcing fibers or plateaus were the dominant wear mechanisms. In the case of formulation GF2, all those described mechanisms were identified in the same proportion, i.e. some peeling, plateaus pull out, and thermal damage, as can be seen in Fig. 14e.

The friction film formed on the cast iron disc for each composite was analyzed in terms of pixel intensity for the entire test. The analysis of tribofilm on the disc is recorded in Fig. S3 (supplementary information) and presented in Fig. 15. In this figure, the spectrum is divided into two parts, namely low temperature (IBT $\leq$100 °C - from braking #1 to #165) and high temperature (IBT $\geq$100 °C - from braking 166 to 275). High-temperature features include fade-recovery and TPS (temperature pressure sensitivity) sections. Overall, all composites exhibited similar tribofilm formation trends throughout the test. For the low-temperature part, the intensity for film formation is lower because of low IBT, and the braking dynamic is controlled by the abrasive and adhesive (due to metallic ingredients) interaction, as evidenced from the grooves formed on the wear track formed on the disc. In the high-temperature part (IBT up to 500 °C); all composites recorded a sudden increase in the tribofilm. At the beginning of the fade 1 section, the amount of tribofilm on the disc was ~140 for GF0 and ~120 $\pm$ 10 for *Grewia optiva* fiber-loaded composite, which suddenly increased to >200 after some braking applications. As temperature easily exceed 300 °C with few braking applications, softening of the organic ingredients (here phenolic resin and natural fibers) begins resulting in more tribofilm formation on the disc.

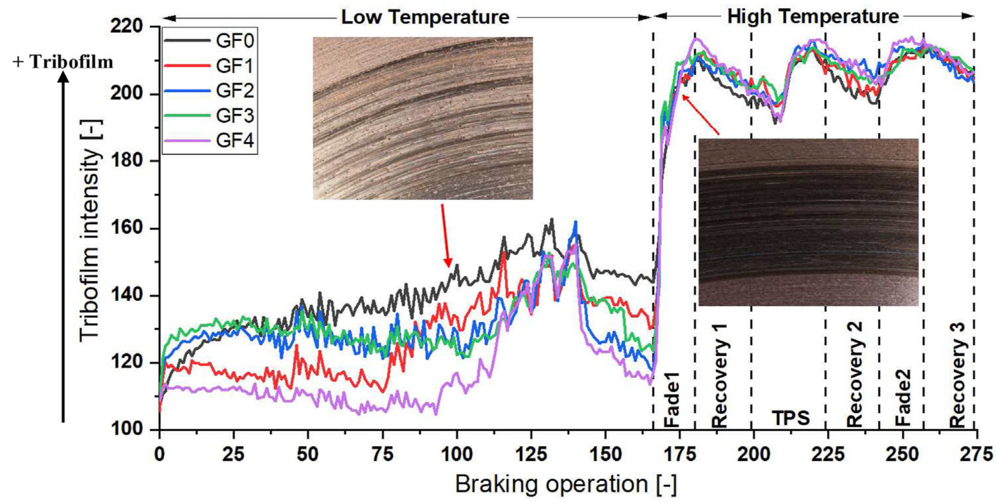

Fig. 15 – Tribofilm amount on the counter disc for each composition.

3.3. *Susceptibility to low frequency brake noise (stick-slip analysis)*

Fig. 16 presents the difference (delta) between static and kinetic coefficient of friction resulting from the stick-slip tests. The larger the box, greater is the variation in friction (i.e. greater delta). The formulation with only ceramic fiber, GF0, exhibited the lowest friction variation, which is a positive indication of fewer propensities to creep groan noise. The addition of natural fiber led to a greater variation in friction, and the formulation with only natural fiber, GF4, had the worst performance in this aspect. However, the hybridization of 7.5% natural fiber with 2.5% ceramic fiber (GF3 formulation) had similar results to the GF0 formulation. The good result of GF3 indicates that a larger amount of natural fiber has a lower noise propensity if combined with ceramic fiber. In this case, 7.5 wt% of the ceramic fiber was replaced by natural fiber without leading to changes in noise sensitivity.

Fig. 17 displays the slip power sum of all tests. The slip power, as presented in section 2.4, is a parameter that measures the magnitude of the stick-slip, i.e. the higher the slip power, the greater the propensity to the creep groans noise. Similar to the results presented earlier, the formulation without ceramic fiber (GF4) showed the worst performance, reaching a total slip power value of 30 Nm/s, and the formulation with only ceramic fiber (GF0) had the best performance (slip power of 7.2 Nm/s). Considering the formulations with both ceramic and natural fibers, GF3 obtained the lowest total slip power, reaching a value of 9.6 Nm/s.

3.4. *Overall performance ranking of the composites*

This section presents the composites' overall effectiveness regarding assessed tribological parameters. The tribological performance patterns of the analyzed composites are complicated. As an illustration, the composite GF2 demonstrated the

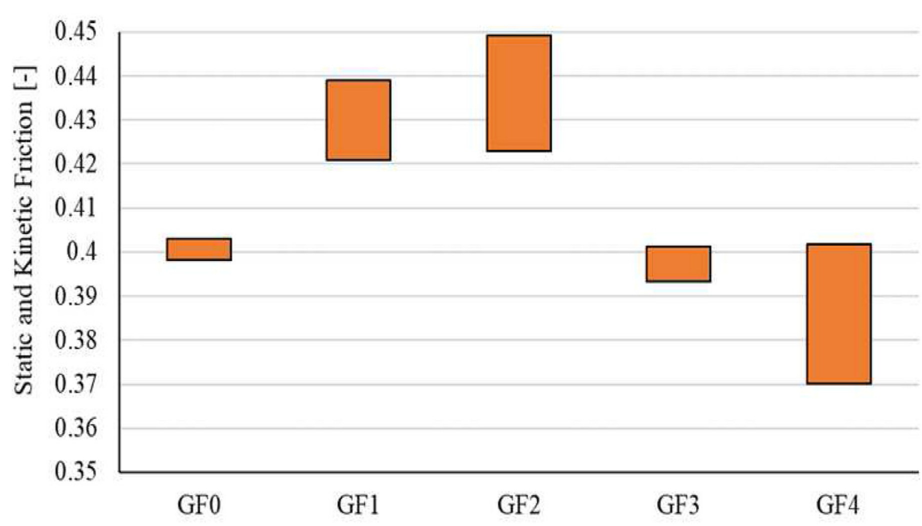

Fig. 16 – Variation (delta) in static (higher) and kinetic (lower) friction for each formulation.

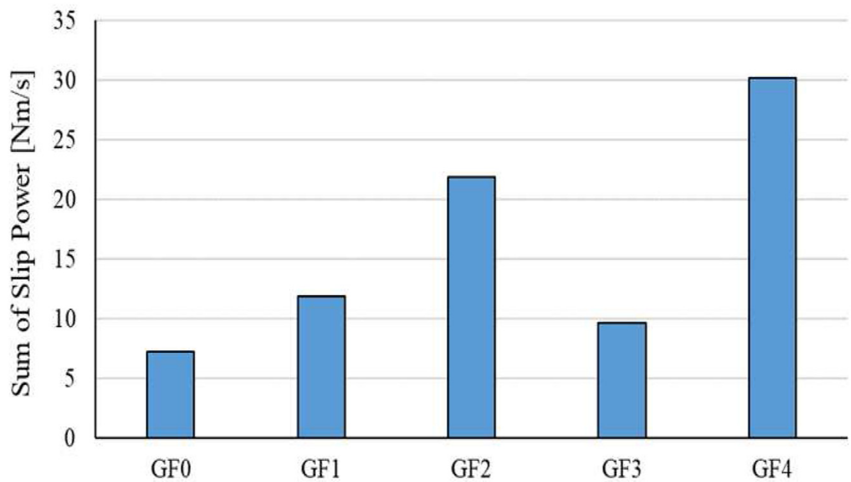

Fig. 17 – Sum of slip power of all tests for each formulation.

Table 5 – The assessment matrix for SAW analysis.

Composites	Attribute 1	Attribute 2	Attribute 3	Attribute 4	Attribute 5	Attribute 6	Attribute 7
	μ_P	μ_{avg}	$\Delta\mu$	Recovery-%	FR-%	SWR	Slip power
GF0	0.42	0.502	0.18	86.13	48.98	3.76×10^{-7}	07.2
GF1	0.41	0.494	0.20	86.77	56.24	3.70×10^{-7}	11.9
GF2	0.44	0.510	0.21	87.19	57.31	4.00×10^{-7}	21.9
GF3	0.41	0.482	0.12	87.75	62.01	3.26×10^{-7}	09.6
GF4	0.42	0.506	0.23	87.78	67.46	3.40×10^{-7}	30.2

greatest μ_P, the lowest wear resistance, and the second-lowest slip power. The composite GF0 has the best slip power and the lowest FR-%, recovery-%, and wear resistance. The FR-% and recovery-% of composite GF4 were the greatest but also had the highest $\Delta\mu$ and slip power values. The results show that not a single composite simultaneously meets the criteria of high μ_P, FR-%, and recovery-%, as well as lowest wear and least $\Delta\mu$. As a result, the SAW approach was used to rank composites to select one that meets all of these contradictory criteria simultaneously. The tribological attributes used in the ranking were chosen as Attribute 1 (μ_P, beneficial), Attribute 2 (μ_{avg}, beneficial), Attribute 3 ($\Delta\mu$, non-beneficial), Attribute 4 (Recovery-%, beneficial), Attribute 5 (FR-%, beneficial), Attribute 6 (SWR, non-beneficial) and Attribute 7 (slip power, non-beneficial). The μ_{avg} and $\Delta\mu$ were taken as the average values for different speeds, as discussed in section 3.2.2. The Recovery-% and FR-% are considered the average of various fade-recovery cycles addressed in section 3.2.3. The results of various performance attributes are presented in Table 5. Normalization was conducted first using Eq. (7), and the final SAW assessment score (A_s) was derived by adding the scores obtained for each performance parameter, as shown in Table 6. The GF3 composite with 7.5 wt% *Grewia optiva* fiber demonstrated the highest value of As = 0.935, indicating that it is the best among all available composite choices in terms of fulfilling the greatest number of performance requirements to provide optimal performance.

Table 6 – SAW assessment score and composites ranking.

	GF0	GF1	GF2	GF3	GF4
Assessment score (A_s)	0.883	0.830	0.794	0.935	0.809
Rank	2	3	5	1	4

4. Conclusions

This work is devoted to providing helpful information about the possibilities offered by *Grewia Optiva*, a natural fiber from the Himalayan region, for developing friction composites used in automotive braking applications. Friction composites based on *Grewia Optiva*-ceramic fiber combinations were fabricated and tribo-evaluated per the SAE J2522 procedure. The friction performance remains comparable between 0.41 and 0.44. Fade resistance, recovery, and specific wear rate could be improved by incorporating *Grewia Optiva* fiber into the formulations. In contrast, susceptibility to low-frequency brake noise could be improved by incorporating ceramic fibers and remains lowest for 10 wt% ceramic fiber added composite. The highest fade resistance and recovery were recorded for the composites having 10 wt% *Grewia Optiva* fiber amount, while friction fluctuations and specific wear rate remain lowest for 7.5 wt% *Grewia Optiva* fiber-loaded composites. The contact plateaus and tribofilm homogeneity analysis agreed with the observed fade-recovery and wear results. The *Grewia Optiva*: ceramic fiber ratio 7.5:2.5 by weight was optimal for reinforcement based on a multi-attribute decision-making approach. The study suggests that combining *Grewia Optiva* fiber and heat-resistant fiber such as ceramic could be applied as reinforcement for developing high-performance brake friction materials. In the future, studies can be conducted to assess the influence of various treatments of *Grewia optiva* fibers in combination with Kevlar, polyacrylonitrile and steel fibers in automotive brake friction composite materials for best performance.

Declaration of competing interest

The authors declare that they have no known competing financial interests or personal relationships that could have appeared to influence the work reported in this paper.

Appendix A. Supplementary data

Supplementary data to this article can be found online at https://doi.org/10.1016/j.jmrt.2023.09.072.

REFERENCES

[1] Wang Y, Yao X, Thorn TDS, Huo S, Porwal H, Newton M, et al. Energy efficient out-of-oven manufacturing of natural fibre composites with integrated sensing capabilities and improved water barrier properties. Compos Sci Technol 2023;239:110062.

[2] Tóthová D, Heglasová M. Measuring the environmental sustainability of 2030 Agenda implementation in EU countries: how do different assessment methods affect results? J Environ Manag 2022;322:116152.

[3] Li W, Ji Z, Dong F. Global renewable energy power generation efficiency evaluation and influencing factors analysis. Sustain Prod Consum 2022;33:438–53.

[4] N. de Beus, M. Carus, M. Barth. Carbon footprint and sustainability of different natural fibres for biocomposites and insulation material. http://eiha.org/media/2019/03/19-03-13-Study-Natural-Fibre-Sustainability-Carbon-Footprint.pdf.

[5] Singh MK, Tewari R, Zafar S, Rangappa SM, Siengchin S. A comprehensive review of various factors for application feasibility of natural fiber-reinforced polymer composites. Results in Materials 2023;17:100355.

[6] Khan MAS, Du J, Malik HA, Anuar MM, Pradana M, Yaacob MRB. Green innovation practices and consumer resistance to green innovation products: moderating role of environmental knowledge and pro-environmental behavior. Journal of Innovation & Knowledge 2022;7:100280.

[7] Ma P, Zhang C, Hong X, Xu H. Pricing decisions for substitutable products with green manufacturing in a competitive supply chain. J Clean Prod 2018;183:618–40.

[8] Rashid B, Leman Z, Jawaid M, Ishak M, AL-Oqla F. Eco-friendly composites for brake pads from agro waste: a review. Encyclopedia of Materials: Composites 2017;3:209–28.

[9] Ahmed MJ, Balaji MAS, Saravanakumar SS, Sanjay MR, Senthamaraikannan P. Characterization of *Areva javanica* fiber-A possible replacement for synthetic acrylic fiber in the disc brake pad. J Ind Text 2019;49:294–317.

[10] Singh T, Singh V, Ranakoti L, Kumar S. Optimization on tribological properties of natural fiber reinforced brake friction composite materials: effect of objective and subjective weighting methods. Polym Test 2023;117:107873.

[11] Ma Y, Liu Y, Ma S, Wang H, Gao Z, Sun J, et al. Friction and wear properties of dumbbell-shaped jute fiber-reinforced friction materials. J Appl Polym Sci 2014;131:40748.

[12] Mustafa A, Abdollah MFB, Shuhimi FF, Ismail N, Amiruddin H, Umehara N. Selection and verification of kenaf fibres as an alternative friction material using Weighted Decision Matrix method. Mater Des 2015;67:577–82.

[13] Fu Z, Suo B, Yun R, Lu Y, Wang H, Qi S, et al. Of eco-friendly brake friction composites containing flax fibers. J Reinforc Plast Compos 2012;31:681–9.

[14] Liu Y, Ma Y, Yu J, Zhuang J, Wu S, Tong J. Development and characterization of alkali treated abaca fiber reinforced friction composites. Compos Interfac 2019;26:67–82.

[15] Ma Y, Wu S, Zhuang J, Tong J, Xiao Y, Qi H. The evaluation of physio-mechanical and tribological characterization of friction composites reinforced by waste corn stalk. Materials 2018;11:901.

[16] Nogueira APG, Gehlen GS, Neis PD, Ferreira NF, Gialanella S, Straffelini G. Rice husk as a natural ingredient for brake friction material: a pin-on-disc investigation. 204272 Wear 2022:494–5.

[17] Ma Y, Wu S, Zhuang J, Tong J, Qi H. Tribological and physio-mechanical characterization of cow dung fibers reinforced friction composites: an effective utilization of cow dung waste. Tribol Int 2019;131:200–11.

[18] Gehlen GS, Neis PD, Barros LY, Poletto JC, Ferreira NF, Amico SC. Tribological performance of eco-friendly friction materials with rice husk. Wear 2022;500–501:204374.

[19] Singh T. Comparative performance of barium sulphate and cement by-pass dust on tribological properties of automotive brake friction composites. Alex Eng J 2023;72:339–49.

[20] Saha D, Sharma D, Satapathy BK. Challenges pertaining to particulate matter emission of toxic formulations and prospects on using green ingredients for sustainable eco-friendly automotive brake composites. Sustainable Materials and Technologies 2023;37:e00680.

[21] Singh T, Aherwar A, Singh V, Ranakoti L, Bhandari P, Lendvai L. Performance optimization of lignocellulosic fiber-reinforced brake friction composite materials using an integrated CRITIC-CODAS-based decision-making approach. Sustainability 2023;15:8880.

[22] Song W, Park J, Choi J, Lee JJ, Jang H. Effects of reinforcing fibers on airborne particle emissions from brake pads. 203996 Wear 2021:484–5.

[23] Monreal-Perez P, Elduque D, López D, Sola I, Yaben J, Clavería I. Full-scale dynamometer tests of composite railway brake shoes including latxa sheep wool fibers. J Clean Prod 2022;379:134533.

[24] Shin MW, Kim YH, Jang H. Effect of the abrasive size on the friction effectiveness and instability of brake friction materials: a case study with zircon. Tribol Lett 2014;55:371–9.

[25] Joo BS, Gweon J, Park J, Song W, Jang H. The effect of the mechanical property and size of the surface contacts of the brake lining on friction instability. Tribol Int 2021;153:106583.

[26] Kalel N, Darpe A, Bijwe J. Propensity to noise and vibration emission of copper-free brake-pads. Tribol Int 2021;153:106651.

[27] Neis PD, Ferreira NF, Poletto JC, Matozo LT, Masotti D. Quantification of brake creep groan in vehicle tests and its relation with stick-slip obtained in laboratory tests. J Sound Vib 2016;369:63–76.

[28] Oberst S, Lai J. A critical review of brake squeal and its treatment in practice. 37th international congress and

exhibition on noise control engineering Inter-Noise conference. Institute of Noise Control Eng 2008;9:670–80.

[29] Wei L, Choy YS, Cheung CS, Jin D. Tribology performance, airborne particle emissions and brake squeal noise of copper-free friction materials. Wear 2020;448–449:203215.

[30] Kalel N, Bhatt B, Darpe A, Bijwe J. Suppression of brake noise and vibration using aramid and Zylon fibers: experimental and numerical study. ACS Omega 2022;7:21946–60.

[31] Monreal P, Oroz J, Gutiérrez K, Ambroj IC. Natural Latxa Sheep Wool as an environmentally friendly substitute for specific organic fibers in railway friction materials: a preliminary approach. Tribol Trans 2021;64:851–63.

[32] Singh T, Pruncu CI, Gangil B, Singh V, Fekete G. Comparative performance assessment of pineapple and Kevlar fibers based friction composites. J Mater Res Technol 2020;9:1491–9.

[33] Ahmadijokani F, Shojaei A, Dordanihaghighi S, Jafarpour E, Mohammadi S, Arjmand M. Effects of hybrid carbon-aramid fiber on performance of non-asbestos organic brake friction composites. Wear 2020;452:203280.

[34] Patnaik A, Kumar M, Satapathy BK, Tomar BS. Performance sensitivity of hybrid phenolic composites in friction braking: effect of ceramic and aramid fibre combination. Wear 2010;269:891–9.

[35] Singha AS, Rana AK, Jarial RK. Mechanical, dielectric and thermal properties of Grewia optiva fibers reinforced unsaturated polyester matrix based composites. Mater Des 2013;51:924–34.

[36] V.K. Thakur, A. S. Singha, M. K. Thakur. Natural cellulosic polymers as potential reinforcement in composites: physicochemical and mechanical studies. Adv Polym Technol, 32, E427-E435.

[37] Rana AK, Potluri P, Thakur VK. Cellulosic *Grewia Optiva* fibres: towards chemistry, surface engineering and sustainable materials. J Environ Chem Eng 2021;9:106059.

[38] Singha AS, Rana AK. A comparative study on functionalization of cellulosic biofibre by graft copolymerization of acrylic acid in air and under microwave radiation. Bioresources 2012;7:2019–37.

[39] Kalauni K, Pawar SJ. Estimation of the physical parameters of Grewia optiva fibers and prediction of sound absorption coefficient with theoretical models. J Nat Fibers 2023;20:2162189.

[40] Singaravelu DL, Vijay R, Filip P. Influence of various cashew friction dusts on the fade and recovery characteristics of non-asbestos copper free brake friction composites. Wear 2019;426–427:1129–41.

[41] Vijay R, Rajan BS, Sathickbasha K, Hariharasakthisudhan P, Singaravelu DL, Manoharan S, et al. Influence of metal sulfide coated steel fibers on the friction and wear performance of brake friction composites. Tribol Int 2022;176:107924.

[42] Neis PD, Ferreira NF, Lorini FJ. Contribution to perform high temperature tests (fading) on a laboratory-scale tribometer. Wear 2011;271:2660–4.

[43] SAE International surface vehicle recommended practice- SAE J2522-Dynamometer Global Brake Effectiveness. AK Master; 2003.

[44] Amirjan M. Microstructure, wear and friction behavior of nanocomposite materials with natural ingredients. Tribol Int 2019;131:184–90.

[45] Poletto JC, Barros LY, Neis PD, Ferreira NF. Analysis of the error in the estimation of the morphology of contact plateaus existing on the surface of brake pads. Tribol Int 2018;126:297–306.

[46] Akbar A, Liew KM. Multicriteria performance evaluation of fiber-reinforced cement composites: an environmental perspective. Composites Part B 2021;218:108937.

[47] Kalel N, Bhatt B, Darpe A, Bijwe J. Copper-free brake-pads: a break-through by selection of the right kind of stainless steel particles. Wear 2021;464:203537.

[48] Kim JW, Joo BS, Jang H. The effect of contact area on velocity weakening of the friction coefficient and friction instability: a case study on brake friction materials. Tribol Int 2019;135:38–45.

[49] Candeo S, Leonardi M, Gialanella S, Straffelini S. Influence of contact pressure and velocity on the brake behaviour and particulate matter emissions. Wear 2023;514–515:204579.

[50] Barros LY, Poletto JC, Bunede D, Flores R, Gehlen G, Neis PD, et al. An experimental study of the transition in the wear regime of brake friction materials. Polym Compos 2021;42:6310–21.

[51] Aranganathan N, Mahale V, Bijwe J. Effects of aramid fiber concentration on the friction and wear characteristics of non-asbestos organic friction composites using standardized braking tests. Wear 2016;354–355:69–77.

[52] Yun R, Filip P, Lu Y. Performance and evaluation of eco-friendly brake friction materials. Tribol Int 2010;43:2010–9.

[53] Tavangar R, Moghadam HA, Khavandi A, Banaeifar S. Comparison of dry sliding behavior and wear mechanism of low metallic and copper-free brake pads. Tribol Int 2020;151:106416.

[54] Lee J-J, Lee J-A, Kwon S, Kim J-J. Effect of different reinforcement materials on the formation of secondary plateaus and friction properties in friction materials for automobiles. Tribol Int 2018;120:70–9.

[55] Kim SJ, Cho MH, Lim DS, Jang H. Synergistic effects of Kevlar pulp and potassium titanate whiskers in the automotive friction material. Wear 2001;251:1484–91.

[56] Gehlen GS, Neis PD, Barros LY, Poletto JC, Ebeling M, Ferreira NF, et al. Tribological behavior of glass/sisal fiber reinforced polyester composites. Polym Compos 2020;41:112–20.

[57] Verma PC, Ciudin R, Bonfanti A, Aswath P, Straffelini G, Gialanella S. Role of the friction layer in the high-temperature pin-on-disc study of a brake material. Wear 2016;346–347:56–65.

[58] Xin X, Xu CG, Qing LF. Friction properties of sisal fibre reinforced resin brake composites. Wear 2007;262:736–41.

[59] Singh T. Utilization of cement bypass dust in the development of sustainable automotive brake friction composite materials. Arab J Chem 2021;14:103324.

[60] Dadkar N, Tomar BS, Satapathy BK, Patnaik A. Performance assessment of hybrid composite friction materials based on flyash-rock fiber combination. Mater Des 2010;31:723–31.

[61] Ma Y, Wu S, Tong J, Zhao X, Zhuang J, Liu Y, et al. Tribological and mechanical behaviours of rattan-fibre-reinforced friction materials under dry sliding conditions. Mater Res Express 2018;5:035101.

[62] Satapathy BK, Patnaik A, Dadkar N, Kolluri DK, Tomar BS. Influence of vermiculite on performance of flyash-based fibre-reinforced hybrid composites as friction materials. Mater Des 2011;32:4354–61.

[63] Singh T. Tribological performance of volcanic rock (perlite)-filled phenolic-based brake friction composites. Journal of King Saud University - Engineering Sciences; 2021. https://doi.org/10.1016/j.jksues.2021.12.010.